Anomalous thermal conductivity across the structural transition in SmBaMn$_2$O$_6$ single crystals

Lu Chen, Ziji Xiang, Colin Tinsman, Qing Huang, K. G. Reynolds, Haidong Zhou, and Lu Li

View Online   Export Citation   CrossMark

Anomalous thermal conductivity across the structural transition in SmBaMn$_2$O$_6$ single crystals

View Online   Export Citation   CrossMark

Lu Chen,[1,a)] Ziji Xiang,[1] Colin Tinsman,[1] Qing Huang,[2] K. G. Reynolds,[2] Haidong Zhou,[2] and Lu Li[1,b)]

AFFILIATIONS

[1]Department of Physics, University of Michigan, Ann Arbor, 450 Church Street, Ann Arbor, Michigan 48109, USA
[2]Department of Physics and Astronomy, The University of Tennessee, Knoxville, Tennessee 37996, USA

a)Electronic mail: chelu@umich.edu
b)Electronic mail: luli@umich.edu

ABSTRACT

To understand whether the enhancement of thermal conductivity could take place at different types of phase transitions, we conduct thermal measurements in SmBaMn$_2$O$_6$ single crystals which have both structural and magnetic phase transitions. In SmBaMn$_2$O$_6$, successive phase transitions in charge, spin, and lattice degrees of freedoms take place at $T_{co1} \sim 362$ K, $T_{co2} \sim 190$ K, and $T_N \sim 175$ K. An enhancement of thermal conductivity is only observed at the structural transition around T_{co1} while it is absent at the structural transition around T_{co2}. One possible explanation is that the spin-phonon coupling in this material strongly modifies the phonon spectra and prevents the evolution of soft-phonon modes around the antiferromagnetic transition T_N, which lies right below T_{co2}. Our study provides a way to look for enhanced thermal conductivity in materials where multiple phase transitions coexist.

Published under license by AIP Publishing. https://doi.org/10.1063/1.5096960

In solid-state materials, structural transitions are always accompanied by changes in other physical properties, such as electrical conductivity, magnetic susceptibility, or thermal conductivity. Enhancement of thermal conductivity across the metal-insulator transition has been reported recently in VO$_2$.[1] VO$_2$ undergoes a first order metal-to-insulator phase transition at around $T_s \sim 340$ K due to a crystal structure and electronic structure change. The thermal conductivity is enhanced by 1 order of magnitude at the transition temperature T_s, which is possibly due to the softening of certain phonon modes at the structural phase transition.[2] It is necessary to further address whether the enhancement of thermal conductivity could also take place at other types of phase transitions and how the ordering states in other degrees of freedom, such as magnetic ordering, could possibly affect it.

Perovskite-type manganites, which have been extensively studied due to their abundant properties originating from the interplay among the charge, spin, orbital, and lattice degrees of freedom, could be one platform to further study this topic.[3] The colossal magnetoresistance (CMR) effect, i.e., the dramatic change of electrical resistivity under a magnetic field, has attracted researchers' attention due to its potential applications in memory device heads and sensors.[4,5] The ferroelectricity driven by the charge-ordering state and the tilting of MnO$_6$ octahedra in layered manganites is also widely studied because of its expected

application in electronic devices such as ferroelectric RAM and capacitors.[6,7] In this article, we focus on the A-site ordered double-perovskite SmBaMn$_2$O$_6$. The A-site ordered SmBaMn$_2$O$_6$ compounds undergo a two-step charge-orbital-order (COO) transition at T_{co1} and T_{co2} as temperature decreases. This material has a first-order structural phase transition at $T_{co1} = 380$ K from the low-temperature tetragonal phase to high-temperature orthorhombic phase.[8] X-ray scattering and electron diffraction reveal a long-range COO phase below T_{co1}.[9,10] The stacking manner of ab plane change from $AABB$- to $ABAB$-type around $T_{co2} = 190$ K is evidenced by X-ray scattering and Raman scattering.[11] At T_{co2}, the space group changes from nonpolar $Pnam$ to polar $P2_1am$, which suggests a ferroelectric transition due to the rearrangement of charge and orbitals at T_{co2}.[7] Yamada *et al.* reported that the antiferromagnetic (AFM) transition happens at $T_N = 175$ K, which is just below T_{co2}.[12]

We conduct electrical transport, magnetic susceptibility, and thermal transport measurements in SmBaMn$_2$O$_6$ single crystals. Both electrical resistance and magnetic susceptibility show an abrupt change accompanied by a narrow hysteresis loop at $T_{co1} \sim 362$ K. Another anomaly takes place between 150 K and 210 K (around T_{co2}) which is manifested by a much broader hysteresis loop. The total thermal conductivity is enhanced by 3–4 times within the metal-insulator-transition (MIT) at T_{co1}, while no obvious enhancement is observed around

T_{co2}. The explanation on the absence of a thermal conductivity peak at the structural transition at T_{co2} is further discussed in this article.

The SmBaMn$_2$O$_6$ single crystals being used in our experiments are grown by the floating zone method.[12] The single crystal is polished into a bar shape for electrical and thermal transport measurement. Sample 1 has a dimension of $0.6 \times 0.65 \times 3$ mm^3 [as shown in Fig. 1(a)]; sample 2 has a dimension of $0.45 \times 0.6 \times 2.5$ mm^3. Sample 3 is cut from the same batch of sample 2, which has a mass of 4.15 mg and is used for magnetization measurement. The crystal structure of SmBaMn$_2$O$_6$ at 300 K is shown in Fig. 1(b), where SmO and BaO layers stack alternatively along the crystal c axis. All the measurements are conducted in a Physical Properties Measurement System (PPMS) DynaCool from Quantum Design.

The experimental setup for the electrical and thermal transport measurement is similar to the setup in Ref. 1. A bar-shape SmBaMn$_2$O$_6$ single crystal is mounted vertically on a sapphire substrate. A resistive heater is attached on top of the sample by the H74F thermal epoxy to provide a thermal gradient inside the [001] plane of the sample. In order to provide better electrical contact with the sample, we evaporate gold contacts on the front surface of the sample and then attach four gold wires on the contacts with silver epoxy. These four gold wires are used for four-probe resistance measurement as well as thermal power measurement. Two type-E thermocouples are thermally linked to the back side of the sample with the thermal joint compound. The whole setup is mounted on top of a self-designed thermal transport puck, which is compatible with the PPMS DynaCool system.
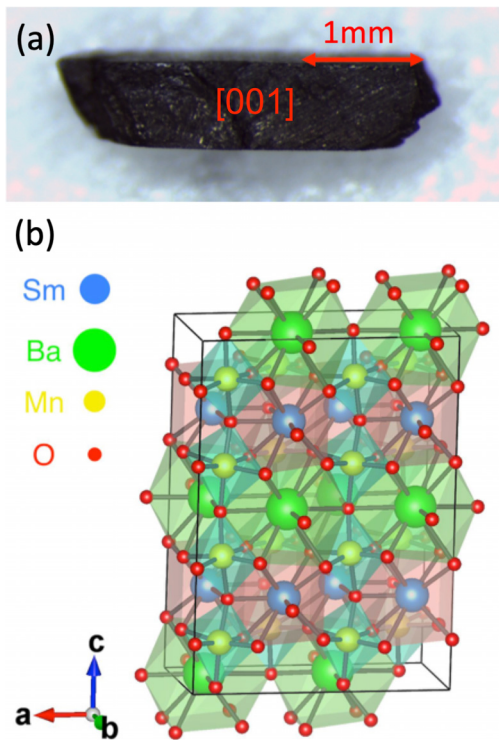

FIG. 1. (a) A polished single crystal of SmBaMn$_2$O$_6$ (sample 1) with the front surface to be [001]. (b) Crystal structure of SmBaMn$_2$O$_6$ at 300 K.[7]

Four-probe resistance measurement is conducted by the Electrical Transport Option (ETO) of PPMS. The thermal power and thermal conductivity are measured by a pulsed power technique.[1,13] A periodic ac current ($f = 0.01$ Hz) is applied through the resistive heater by a Keithley 6221 DC and AC current source to generate a thermal gradient across the sample. The thermal power is measured through two of the electrical contacts by a Keithley 2182A nanovoltmeter. The voltage across the two thermocouples is read by another Keithley 2182A nanovoltmeter, which could be used to calculate the temperature gradient across the sample. During the thermal transport measurement, the sample temperature is swept with a speed of 0.1 K/min. Magnetization is measured using the Vibrating Sample Magnetometer (VSM) of PPMS. For the temperature dependent measurement, we first cool the sample down to 100 K without applying any magnetic field. Then, we apply a magnetic field of 3 T at 100 K and measure the magnetization during warm up and cooldown.

Figure 2(a) shows the four-probe resistance measured in the SmBaMn$_2$O$_6$ sample 1 and sample 2. A slowly varying ac current is applied inside the [001] plane of the sample. Sample 1 undergoes an MIT at $T_{co1} \sim 362$ K with a resistance increase of about 20 times during cooldown. The resistance of sample 2 only increases about 10 times at $T_{co1} \sim 354$ K. Both samples show a steep change in resistance with a thermal hysteresis loop at T_{co1} which is clear evidence of a first-order phase transition.[12] The difference between the transition temperature T_{co1} during warm up and cooldown is around 6 K. The difference in the transition temperature between sample 1 and 2 could be caused by the valence distribution of Mn ions. The charge-ordering is from the mixed valence of the two Mn ions, one is +3 and the other one is +4. The charge ordering temperature is very sensitive to the
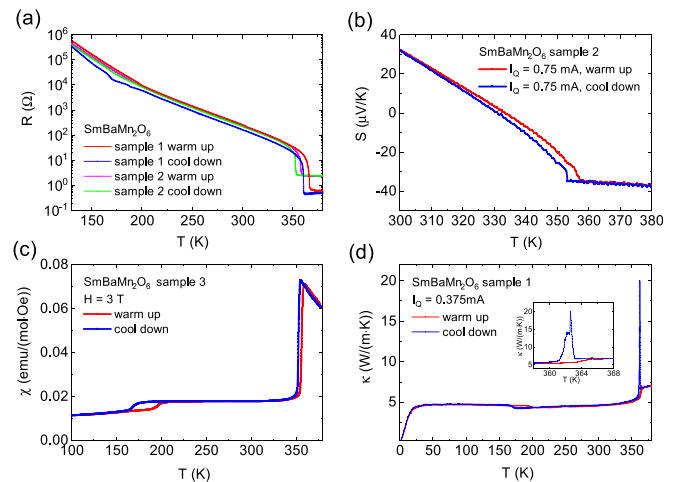

FIG. 2. (a) Four-probe resistance R vs T in SmBaMn$_2$O$_6$ sample 1 and 2. The current is applied in the [001] plane. (b) Seebeck coefficient S vs T in SmBaMn$_2$O$_6$ sample 2. The sample temperature was swept at a rate of 0.1 K/min. (c) Temperature dependence of magnetic susceptibility in SmBaMn$_2$O$_6$ sample 3 taken with H = 3 T. (d) Measured total thermal conductivity κ_{tot} vs T in SmBaMn$_2$O$_6$ sample 1 with a slower sweeping speed of temperature ($\sim$0.02 K/min) around T_{co1}. The inset figure is a zoom in of κ_{tot} around T_{co1}, which shows that the thermal conductivity increases about 4 times across T_{co1} during cooling down. In (a)–(d), red (magenta) curves denote warming up while blue (green) curves denote cooling down.

valence distribution, which means that a slight deviation from this +3/+4 valence combination could change or even eliminate the charge ordering transition.[14,15] The deviation of the valence from +3/+4 is reflected by the inhomogeneous oxygen deficiency in the different parts of the as-grown crystals during the melting process. Upon further cooling, another anomaly is observed between 150 K and 210 K (around $T_{co2} \simeq 190$ K) in resistance, which is consistent with the observation in Ref. 12. The temperature dependent Seebeck coefficient changes sign at 330 K and reaches an almost constant value of $-34\,\mu$V/K at T_{co1} when entering the metallic state [as shown in Fig. 2(b)]. The temperature dependent magnetic susceptibility shows a steep change accompanied by a narrow hysteresis loop at T_{co1} [as shown in Fig. 2(c)], while a much broader hysteresis loop is observed between 160 K and 210 K (around T_{co2}). Nakajima et al. have reported that the magnetization curve has a broad peak at around 250 K in the pulverized sample, which is assigned to the AFM transition.[8,16] However, this peak is strongly suppressed in our measurement as well as experiments of Yamada et al., which indicates a strong dependence of sample properties on the system size.

The temperature dependent total thermal conductivity between 2 K and 380 K of sample 1 is shown in Fig. 2(d). The thermal conductivity increases about 50% from a low-temperature insulating state to a high-temperature metallic state at T_{co1}. The inset of Fig. 2(d) shows that the thermal conductivity is enhanced by 3–4 times within the MIT during cooldown, while the enhancement during warm-up is much weaker. Between 150 K and 210 K, another anomaly which is accompanied by a hysteresis loop is observed on the thermal conductivity. Figure 3(a) shows the zoom-in of the total thermal conductivity between 2 K and 300 K. Recently, the enhancement of thermal conductivity within the MIT of oxides has been reported in the VO$_2$ single crystals, which is claimed to be related to the soft phonons at the

structural transition.[1] Although the phase transitions at T_{co1} and T_{co2} are both accompanied by structural transitions in SmBaMn$_2$O$_6$, no obvious enhancement of thermal conductivity is observed around T_{co2}. Instead, the thermal conductivity shows a dip around T_{co2} before entering the AFM state.

We vary the temperature sweeping speed as well as the heater current to further study the thermal conductivity peak within the MIT. Figures 3(b) and 3(c) show the total thermal conductivity measured in sample 1 with a temperature sweeping speed of 0.1 K/min (0.02 K/min). The thermal conductivity peak is more prominent with a slower sweeping speed of temperature because a faster sweeping speed of temperature will smear out the enhancement effect that only happens in a very narrow temperature range. The total thermal conductivity shows a nonmonotonic dependence on the heater current, which is in contrast to the monotonic behavior observed in the VO$_2$ single crystals.[1] Furthermore, the thermal conductivity shows comparable enhancement during both warm up and cooldown in VO$_2$, while it only shows obvious enhancement during cooldown in SmBaMn$_2$O$_6$. Figure 3(d) shows the total thermal conductivity measured in sample 2 with a temperature sweeping speed of 0.1 K/min. The thermal conductivity peak in sample 2 is lower than that in sample 1.

First of all, we ask if thermal conductivity peaks observed at the structural transition $T_{co1} \sim 362$ K arise from the latent heat. Latent heat is released at the first-order structural transition. This heat leads to a sudden rise in the overall temperature, which changes the overall trend in the thermocouple voltage raw data. As we explained in the method part, we take the difference of this voltage signal between the "sample heater on" and "sample heater off" to infer the thermal conductivity, which actually excludes the effect of the latent heat because the latent heat affects both data of sample heater on and sample heater off. More importantly, we may estimate the latent heat releasing power across T_{co1} by assuming that the latent heat released at the transition is on the same order of magnitude as VO$_2$.[17] For the most significant peak observed in sample 1 [Fig. 3(c)], we find that the latent heat releasing power is only less than 1% of that of the sample heater. As a result, we do not think that the latent heat is the main driving force of the sharp peak in the thermal conductivity.

Now what is the origin of the thermal conductivity peak at T_{co1}? We note that the thermal conductivity peak at the MIT in the VO$_2$ single crystal can likely be explained by a soft optical phonon mode which has been observed by neutron scattering.[18] VO$_2$ undergoes a first order MIT at around 340 K from the insulating monoclinic phase to the metallic rutile phase as temperature increases. Generally, at the structural transition, acoustic phonon modes soften because of the instability of the lattice structure. The decrease of the phonon energy is overcompensated by a large increase in phonon population and its group velocity, which strongly enhances the thermal conductivity at the structural transition. In SmBaMn$_2$O$_6$, the thermal conductivity peak at T_{co1} can likely be explained with the same scenario.

The absence of such enhancement around T_{co2} may come from the adjacency between the structural transition at $T_{co2} \sim 190$ K and the AFM ordering at $T_N \sim 175$ K. First-principles calculations suggest strong spin-phonon coupling in perovskite-type manganites like SrMnO$_3$ and Sr$_{1-x}$Ba$_x$MnO$_3$.[19–21] As the Ba concentration increases, one optical phonon mode rapidly softens at room temperature while other phonon modes remain unchanged. The infrared optical and inelastic x-ray scattering spectra confirm that only the soft phonon
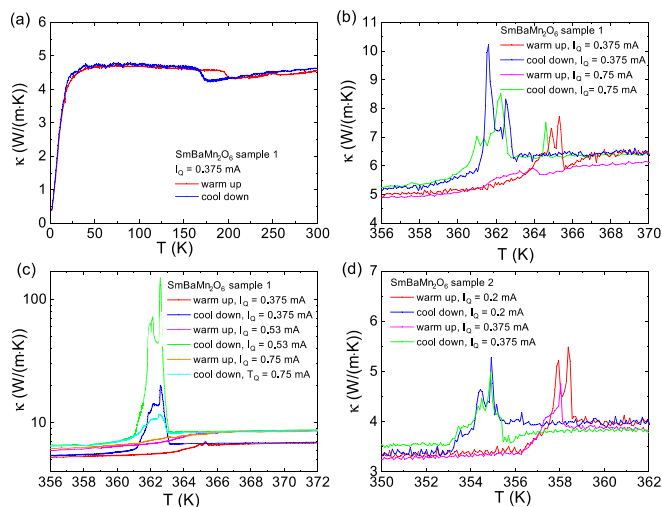

FIG. 3. (a) Measured total thermal conductivity κ_{tot} vs T in SmBaMn$_2$O$_6$ sample 1 below 300 K. (b) Total thermal conductivity κ_{tot} vs T in SmBaMn$_2$O$_6$ sample 1 with different heater currents. The temperature sweeping speed is 0.1 K/min around T_{co1}. (c) Total thermal conductivity κ_{tot} vs T in SmBaMn$_2$O$_6$ sample 1 with different heater currents. The temperature sweeping speed is 0.02 K/min around T_{co1}. (d) Total thermal conductivity κ_{tot} vs T in SmBaMn$_2$O$_6$ sample 2 with different heater currents. The temperature sweeping speed is 0.1 K/min around T_{co1}.

modes show remarkable variation with AFM transition for all doping levels while other phonon modes are almost temperature independent. As temperature decreases, the continuous softening of this optical phonon is suppressed by the onset of the AFM phase. The soft phonon mode first hardens below T_N and then resoftens at a much lower temperature. Furthermore, the soft-phonon-mode frequency is even modified above T_N because of the strong AFM fluctuation near T_N, which also results in the disappearance of the thermal conductivity peak at T_{co2}.[20] This nonmonotonic temperature dependence of soft-phonon-mode frequency can be explained by considering the spin-phonon coupling

$$\omega_{TO1}^2 = \omega_0^2 + \lambda \langle \mathbf{S}_i \cdot \mathbf{S}_j \rangle, \tag{1}$$

where ω_0 is a phonon frequency without magnetism, λ is a coupling constant, and $\langle \mathbf{S}_i \cdot \mathbf{S}_j \rangle$ is the nearest-neighbor spin correlation function.[22,23] By fitting the theoretical model with the infrared spectra data, the spin-phonon coupling constant in $Sr_{1-x}Ba_xMnO_3$ ($x = 0.3$) is 500 times stronger than that in $EuTiO_3$. We also observe that the total thermal conductivity of $SmBaMn_2O_6$ shows a dip at $T_s = 175\,K$ (200 K) during cooling down (warming up) and starts to increase as the temperature becomes lower. This is similar to the observations in other magnetic materials or CMR manganites, where $d\kappa/dT$ changes sign upon entering a Ferromagnetic (FM) or AFM transition.[24–28] These features can also be attributed to the strong spin-phonon coupling in these systems, where the critical scattering of thermal phonons on spin fluctuations leads to a dip on κ.[29–32] In order to fully understand the thermal conductivity behavior in $SmBaMn_2O_6$, other measurement methods, as well as first-principles calculation, are needed to illustrate the phonon spectra.

$SmBaMn_2O_6$ single crystals have a MIT above room temperature at $T_{co1} \sim 362\,K$. Such a high T_{co1} value is very attractive from the aspect of device application.[16] The huge thermal conductivity peak provides a path to efficiently conduct the heat out of the device, which suggests a possible way to achieve thermal management in such kinds of materials. The soft-phonon modes in this material suggest a potential application in temperature-tunable thermal switches.[33]

In summary, we conduct electrical transport, magnetic susceptibility, and thermal transport measurements in $SmBaMn_2O_6$ single crystals. Both electrical resistance and magnetic susceptibility show an abrupt change accompanied by a narrow hysteresis loop at $T_{co1} \sim 362\,K$. Upon further cooling down, another anomaly takes place between 150 K and 210 K (around T_{co2}) which is manifested by a much broader hysteresis loop. The total thermal conductivity is enhanced by 3–4 times within the MIT at T_{co1}, while no obvious peak is observed around T_{co2}. The enhancement of thermal conductivity within the structural transition at T_{co1} is likely due to the phonon softening. Around T_N, the spin-phonon coupling in this material strongly modifies the phonon spectra and prevents the evolution of soft-phonon modes. The hardening of soft-phonon modes around T_N could cause the absence of the thermal conductivity peak around T_{co2}, which lies right above T_N.

REFERENCES

[1]L. Chen, Z. Xiang, C. Tinsman, T. Asaba, Q. Huang, H. Zhou, and L. Li, Appl. Phys. Lett. **113**, 061902 (2018).
[2]H. Aramberri, R. Rurali, and J. Íñiguez, Phys. Rev. B **96**, 195201 (2017).
[3]Y. Tokura and N. Nagaosa, Science **288**, 462 (2000).
[4]E. Dagottoa, T. Hottab, and A. Moreo, Phys. Rep. **344**, 1 (2001).
[5]Y. Tokura, Rep. Prog. Phys. **69**, 797 (2006).
[6]Y. Tokunaga, T. Lottermoser, Y. Lee, R. Kumai, M. Uchida, T. Arima, and Y. Tokura, Nat. Mater. **5**, 937 (2006).
[7]H. Sagayama, S. Toyoda, K. Sugimoto, Y. Maeda, S. Yamada, and T. Arima, Phys. Rev. B **90**, 241113(R) (2014).
[8]D. Akahoshi, M. Uchida, Y. Tomioka, T. Arima, Y. Matsui, and Y. Tokura, Phys. Rev. Lett. **90**, 177203 (2003).
[9]M. Uchida, D. Akahoshi, R. Kumai, Y. Tomioka, T.-H. Arima, Y. Tokura, and Y. Matsui, J. Phys. Soc. Jpn. **71**, 2605 (2002).
[10]D. Morikawa, K. Tsuda, Y. Maeda, S. Yamada, and T. Arima, J. Phys. Soc. Jpn. **81**, 093602 (2012).
[11]D. Akahoshi, Y. Okimoto, M. Kubota, R. Kumai, T. Arima, Y. Tomioka, and Y. Tokura, Phys. Rev. B **70**, 064418 (2004).
[12]S. Yamada, Y. Maeda, and T.-H. Arima, J. Phys. Soc. Jpn. **81**, 113711 (2012).
[13]D. Zhao, X. Qian, X. Gu, S. A. Jajja, and R. Yang, J. Electron. Packag. **138**(4), 040802 (2016).
[14]W. Schuddinck, G. Van Tendeloo, C. Martin, M. Hervieu, and B. Raveau, J. Alloys Compd. **333**, 13 (2002).
[15]Y. G. Zhao, W. Cai, J. Zhao, X. P. Zhang, B. S. Cao, M. H. Zhu, L. W. Zhang, S. B. Ogale, T. Wu, T. Venkatesan, L. Lu, T. K. Mandal, and J. Gopalakrishnan, Phys. Rev. B **65**, 144406 (2002).
[16]T. Nakajima and Y. Ueda, J. Appl. Phys. **98**, 046108 (2005).
[17]C. N. Berglund and H. J. Guggenheim, Phys. Rev. **185**, 1022 (1969).
[18]J. D. Budai, J. Hong, M. E. Manley, E. D. Specht, C. W. Li, J. Z. Tischler, D. L. Abernathy, A. H. Said, B. M. Leu, L. A. Boatner, R. J. McQueeney, and O. Delaire, Nature **515**, 535 (2014).
[19]G. Giovannetti, S. Kumar, C. Ortix, M. Capone, and J. van den Brink, Phys. Rev. Lett. **109**, 107601 (2012).
[20]H. Sakai, J. Fujioka, T. Fukuda, M. S. Bahramy, D. Okuyama, R. Arita, T. Arima, A. Q. R. Baron, Y. Taguchi, and Y. Tokura, Phys. Rev. B **86**, 104407 (2012).
[21]S. Kamba, V. Goian, V. Skoromets, J. Hejtmánek, V. Bovtun, M. Kempa, F. Borodavka, P. Vaněk, A. A. Belik, J. H. Lee, O. Pacherová, and K. M. Rabe, Phys. Rev. B **89**, 064308 (2014).
[22]T. Katsufuji and H. Takagi, Phys. Rev. B **64**, 054415 (2001).
[23]J. Hong, A. Stroppa, J. Íñiguez, S. Picozzi, and D. Vanderbilt, Phys. Rev. B **85**, 054417 (2012).
[24]F. B. Lewis and N. H. Saunders, J. Phys. C **6**, 2525 (1973).
[25]J. L. Cohn, J. J. Neumeier, C. P. Popoviciu, K. J. McClellan, and T. Leventouri, Phys. Rev. B **56**, R8495(R) (1997).
[26]D. W. Visser, A. P. Ramirez, and M. A. Subramanian, Phys. Rev. Lett. **78**, 3947 (1997).
[27]K. H. Kim, M. Uehara, C. Hess, P. A. Sharma, and S.-W. Cheong, Phys. Rev. Lett. **84**, 2961 (2000).
[28]M. Tachibana and E. Takayama-Muromachi, Appl. Phys. Lett. **92**, 242507 (2008).
[29]K. Kawasaki, Prog. Theor. Phys. **29**, 801 (1963).
[30]H. Stern, J. Phys. Chem. Solids **26**, 153 (1965).
[31]G. S. Dixon and D. Walton, Phys. Rev. **185**, 735 (1969).
[32]P. A. Sharma, J. S. Ahn, N. Hur, S. Park, S. B. Kim, S. Lee, J.-G. Par, S. Guha, and S.-W. Cheong, Phys. Rev. Lett. **93**, 177202 (2004).
[33]G. Venkataraman, Bull. Mater. Sci. **1**, 129 (1979).